nature astronomy

LETTERS

https://doi.org/10.1038/s41550-019-0903-z

Diffuse X-ray emission around an ultraluminous X-ray pulsar

Andrea Belfiore[1*], Paolo Esposito[1,2], Fabio Pintore[1], Giovanni Novara[2], Ruben Salvaterra[1], Andrea De Luca[1,3], Andrea Tiengo[1,2,3], Patrizia Caraveo[1], Felix Fürst[4], Gian Luca Israel[5], Danilo Magistrali[6], Martino Marelli[1], Sandro Mereghetti[1], Alessandro Papitto[5], Guillermo A. Rodríguez Castillo[5], Chiara Salvaggio[7,8], Luigi Stella[5], Dominic J. Walton[9], Anna Wolter[8] and Luca Zampieri[10]

Ultraluminous X-ray sources (ULXs) are extragalactic X-ray emitters located off-centre of their host galaxy and with a luminosity in excess of a few 10^{39} erg s^{-1}, if emitted isotropically[1,2]. The discovery of periodic modulation revealed that in some ULXs the accreting compact object is a neutron star[3–7], indicating luminosities substantially above their Eddington limit. The most extreme object in this respect is NGC 5907 ULX-1 (ULX1), with a peak luminosity that is 500 times its Eddington limit. During a Chandra observation to probe a low state of ULX1, we detected diffuse X-ray emission at the position of ULX1. Its diameter is 2.7 ± 1.0 arcsec and contains 25 photons, none below 0.8 keV. We interpret this extended structure as an expanding nebula powered by the wind of ULX1. Its diameter of about 200 pc, characteristic energy of ~1.9 keV and luminosity of ~2×10^{38} erg s^{-1} imply a mechanical power of 1.3×10^{41} erg s^{-1} and an age of ~7×10^{4} yr. This interpretation suggests that a genuinely super-Eddington regime can be sustained for timescales much longer than the spin-up time of the neutron star powering the system. As the mechanical power from a single ULX nebula can rival the injection rate of cosmic rays of an entire galaxy[8], ULX nebulae could be important cosmic ray accelerators[9].

NGC 5907 is a nearly edge-on (inclination of 87° (ref. [10])) spiral galaxy at a distance $D = 17.1$ Mpc (ref. [11]). Its source NGC 5907 ULX-1 (henceforth ULX1), with a peak X-ray luminosity $\gtrsim10^{41}$ erg s^{-1}, is driven by an accreting neutron star with a spin period of ~1 s (ref. [5]). During an X-ray multi-instrument campaign to study its behaviour, ULX1 dimmed its flux by a factor >50 (Fig. 1) and, on 7 November 2017, Chandra observed the field of ULX1 with its Advanced CCD Imaging Spectrometer for 52 ks. A source at the position of ULX1 was detected at a 7.7σ confidence level (Fig. 2). Since the number of collected photons is rather low, we made extensive use of simulations to assess the robustness of the findings and estimate the parameters characterizing the source. For our analysis, we considered the events between 0.3 and 7.0 keV falling within 3 arcsec from the coordinates of ULX1, totalling 25 photons (3.6 of which are expected from background alone). The emission appears to be extended and indeed we verified that the photon distribution in the detector is not consistent with the point-spread function (PSF) of the telescope: we can reject a point-like nature of this source at the 5σ confidence level. We modelled the emission with a disk profile with uniform surface brightness and estimated the disk radius to be $R_d = 1.35 \pm 0.50$ arcsec. We found no indication of an excess of brightness at the centre of the source. To set an upper limit on the flux of ULX1 (the point-like component of the source), we selected the photons in the innermost part of the PSF, within 0.5 arcsec, to compute a Poisson upper limit on the count rate. Assuming a power-law spectrum with photon index $\Gamma = 2$ and an absorbing column $N_H = 5.3\times10^{21}$ cm^{-2} (the value measured when the source was bright[5]), we obtained an upper limit on the point source unabsorbed flux in the 0.3–7.0 keV energy range of $F_X < 3.4\times10^{-15}$ erg cm^{-2} s^{-1} at the 90% confidence level. This corresponds to a limit on the isotropic X-ray luminosity $L_X < 1.2\times10^{38}$ erg s^{-1}, lower than the Eddington luminosity ($L_{Edd} \approx 1.7\times10^{38}$ erg s^{-1}) for a 1.4 $M_\odot$ neutron star.

The diffuse emission at the position of ULX1 can be either an effect of the propagation of the high-energy emission of the ULX through a thick dust layer in NGC 5907 or the intrinsic emission of an extended structure physically associated to ULX1. X-ray dust-scattering could produce a halo of the size we observe only if ULX1 were located at least 6 kpc behind the dominant scattering layer. However, in this case, given the high inclination and gas distribution of NGC 5907[12], standard assumptions imply an X-ray absorption along our line of sight much higher than the column density we derive from the X-ray spectrum of ULX1[5] (see the Supplementary Information for a discussion and Supplementary Fig. 4). We therefore concentrate on the hypothesis of nebular emission surrounding the ULX. At the distance of NGC 5907, the radius of the X-ray nebula is $R = 112 \pm 42$ pc. For a collisionally ionized diffuse gas and absorption $N_H = (1.3^{+4.0}_{-1.2})\times10^{21}$ cm^{-2}, we estimate a temperature T corresponding to $k_BT = 1.9^{+2.3}_{-0.8}$ keV (where k_B is the Boltzmann constant), an unabsorbed flux $F_X = (6.1^{+6.1}_{-2.5})\times10^{-15}$ erg cm^{-2} s^{-1} and a luminosity $L_X = (2.1^{+2.1}_{-0.9})\times10^{38}$ erg s^{-1}. A diffuse flux consistent with L_{Edd} may suggest that the Eddington-limited radiation from a neutron star is being Compton scattered by the wind. However, given that $\sigma_T \times N_H < 4\times10^{-4}$ (where σ_T is the Thompson cross-section), >99% of the observed emission is unscattered. If this were the remnant of a supernova, its energy would be $E_{sn} > 10^{53}$ erg (ref. [13]), corresponding to a hypernova explosion. This is expected to

[1]INAF–Istituto di Astrofisica Spaziale e Fisica Cosmica di Milano, Milano, Italy. [2]Scuola Universitaria Superiore IUSS Pavia, Pavia, Italy. [3]INFN–Istituto Nazionale di Fisica Nucleare, Pavia, Italy. [4]ESAC–European Space Astronomy Centre, Science Operations Departement, Madrid, Spain. [5]INAF–Osservatorio Astronomico di Roma, Monteporzio Catone, Italy. [6]Universidad Pontificia Comillas Madrid–ICAI, Madrid, Spain. [7]Department of Physics G. Occhialini, University of Milano–Bicocca, Milano, Italy. [8]INAF–Osservatorio Astronomico di Brera, Milano, Italy. [9]Institute of Astronomy, University of Cambridge, Cambridge, UK. [10]INAF–Osservatorio Astronomico di Padova, Padova, Italy. *e-mail: andrea.belfiore@inaf.it

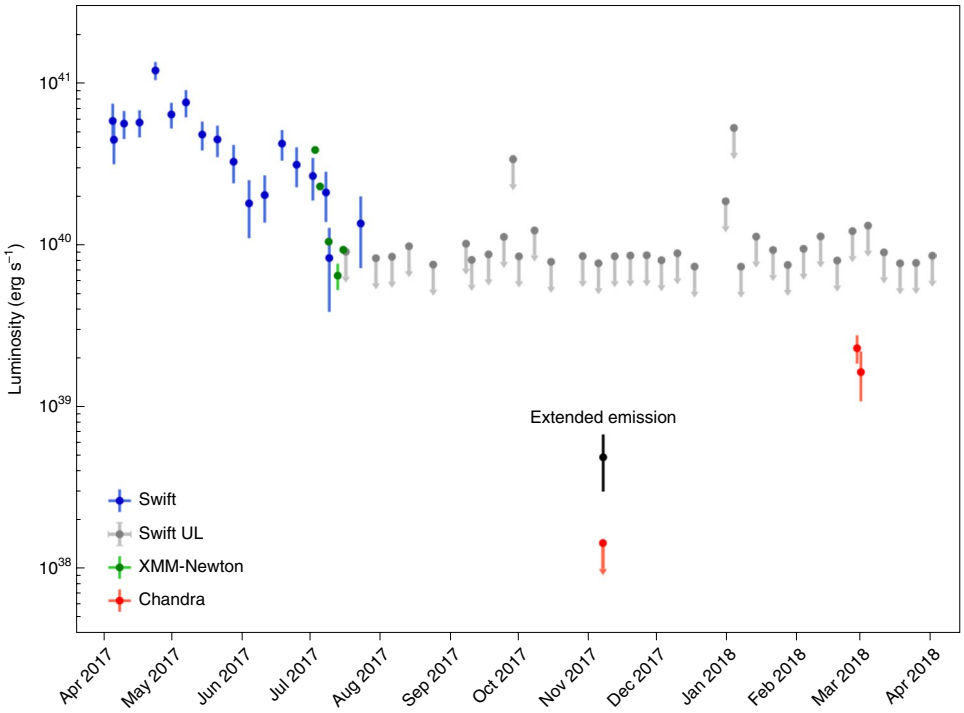

Fig. 1 | Multi-instrument soft X-ray light curve of NGC 5907 ULX-1 since April 2017, when the Swift monitoring resumed. The *y* axis shows the luminosity in the 0.2–10 keV energy range, assuming a distance $D = 17.1$ Mpc. In July 2017, when XMM-Newton started observing, the source left its regularly modulated high state[48]. After ULX1 fell below the detection limit of Swift, Chandra observed ULX1 in its low state in November 2017 and obtained an upper limit (red downward arrow), assuming a power-law spectrum with index $\Gamma = 2$. The luminosity of the diffuse source (extended X-ray emission) associated to ULX1 assumes a collisional plasma (apec) spectrum with $k_{\rm B}T = 1.9^{+2.3}_{-0.8}$ keV (black). The grey arrows and blue points represent Swift upper limits (UL) and detections, respectively, assuming a broken power law spectrum, as modelled by XMM-Newton in the high state of ULX1[5]. New Chandra observations (red points) taken in March 2018 found ULX1 in an intermediate state. All the error bars show uncertainties at the 90% confidence level.

produce a black hole[14] but, in exotic scenarios, it could leave behind a neutron star[15].

Nebular emission has been observed around several ULXs at optical and radio wavelengths[1,2,16–20]. These nebulae (often referred to as bubbles) are generally attributed to shocks created by outflows from the binary system interacting with the surrounding medium and show some common traits: diameter of ~200–400 pc, expansion speed of ~100–200 km s^{-1}, characteristic age (derived from the expansion velocity and the size of the nebula) of ~1 Myr, and mechanical power ~10^{39}–10^{40} erg s^{-1}. Here we explore whether a quasi-isotropic wind shocking the interstellar medium (ISM)[21,22] can account for the extended X-ray emission around ULX1. As the bubble expands over time t with a radius $R \propto t^{3/5}$ (ref. [21]), the ISM accumulates just behind this external shock. The wind, faster than the shock, also accumulates in another region closer to the source. Assuming that the X-ray emission comes from the outer region, pressure equilibrium at the shock boundary provides an estimate of the shock velocity $v_{\rm sh} = \sqrt{\frac{5\,k_{\rm B}T}{16\,m_{\rm p}}} \approx 1,000\,{\rm km\,s^{-1}}$ (where $k_{\rm B}T$ comes from the spectral fit and $m_{\rm p}$ is the proton mass), which entails an age of the bubble $\tau = \frac{3}{5}\frac{R}{v_{\rm sh}} = \left(6.7^{+3.1}_{-2.8}\right) \times 10^4$ yr. This value is much larger than the spin-up timescale of the neutron star that powers the system, 40 yr (ref. [5]). We also derived an estimate of the ISM density (see Methods) as $n_{\rm ISM} \approx 0.08\,{\rm cm^{-3}}$ and of the mechanical power carried by the wind, $L_{\rm w} = \left(1.3^{+9.8}_{-1.0}\right) \times 10^{41}$ erg s^{-1}, not far from the value of 5×10^{40} erg s^{-1} estimated for the bubble S26 in NGC 7793[23,24]. If this mechanical power were sustained for ~7×10^4 yr, then, assuming a typical accretion efficiency onto a neutron star of 17%, ~0.9 $M_\odot$ should have been accreted to provide enough energy to sustain the nebula. Because the wind carries mechanical power to the nebula, if a large mass has been accreted onto the neutron star, and the mass lost by the system cannot exceed a few 10 $M_\odot$, then we obtain a speed of the wind $v_{\rm w} \gtrsim 0.1c$, where c is the speed of light. This value is consistent with the outflows observed from other ULXs[25–27].

NGC 5907 has been observed in H_α with the Kitt Peak National Observatory 0.9 m telescope in May 1995[28]. The high level of contamination from star forming regions and the limited angular resolution (~1 arcsec) hamper a detection of a counterpart in H_α to the nebula around ULX1. NGC 5907 ULX-1 has been observed in radio at 5 GHz with the Very Large Array in May 2012[29], detecting no point source down to a flux density of 20 μJy. The radio emission expected from the hot X-ray-emitting plasma is much fainter than this limit (see the Supplementary Information for a discussion). However, because efficient radiative cooling would have boosted the radio emission to ~240 μJy (refs. [30,31]), this limit confirms our adiabatic approximation and justifies the large ratio $L_{\rm w}/L_{\rm X}$.

Observing an X-ray bubble around a ULX requires a number of favourable circumstances: a bubble with the right surface brightness and size to be detectable as extended; a ULX dim enough not to outshine the bubble; and a sensitive observation carried out with an instrument with good angular resolution (see the Supplementary Information for a quantitative discussion and Supplementary Fig. 3). This might explain why no similar structures are commonly observed (with the notable exception of NGC 7793 S26[23], which, however, has no associated ULX). Indeed, two follow-up observations with Chandra performed between 27 February 2018 and 1 March 2018 for a combined exposure of 50 ks failed to detect the bubble, as ULX1 raised its luminosity to 4×10^{39} erg s^{-1}.

The recent discovery of TeV emission from the Galactic microquasar SS 433[9], in many ways reminiscent of ULXs[32], suggests that

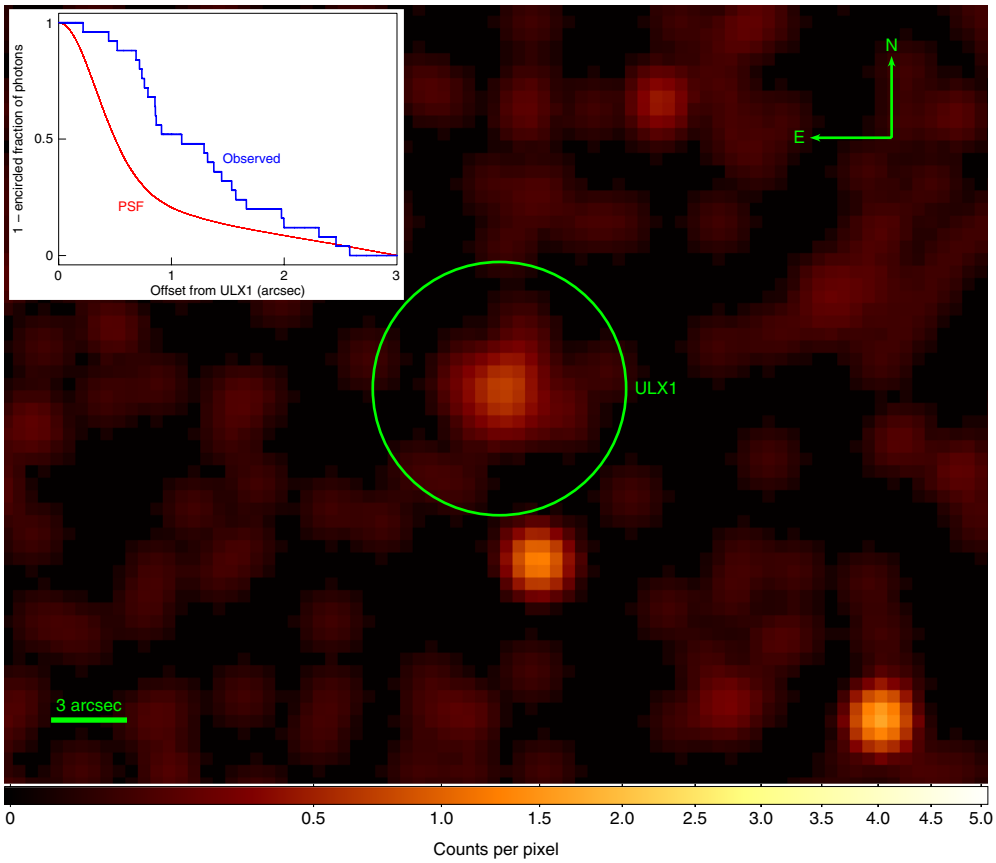

Fig. 2 | X-ray sky map between 0.3 and 7.0 keV of the region around the direction of NGC 5907 ULX-1 as observed by Chandra in November 2017. Nearby sources are not significantly extended and their radial profile can be compared by eye with that of the diffuse emission. In the latter, no clear enhancement in brightness appears at the centre of the source, indicating a discrepancy from the instrument PSF. The green circle, with a radius of 5 arcsec, is centred on the position of ULX1. The scale is in counts per pixel, whose side measures 0.5 arcsec, after smoothing the image through a 2D Gaussian kernel with $\sigma_{\mathrm{Gauss}} = 1.5$ pixels. The inset shows a comparison between the PSF (as obtained from simulations, including background) and the observed radial distribution of the events (the *y* axis represents the fraction of events falling outside a certain radius). We can reject the hypothesis that the source is point-like with a confidence level of 5σ (*P* value $= 3 \times 10^{-7}$). See Supplementary Fig. 1 for a broader and unsmoothed version of this map.

strong shocks associated to ULXs contribute to the cosmic-ray acceleration. Indeed, the mechanical power of the bubble of ULX1 is comparable to the cosmic-ray injection rate for a whole galaxy[8]. Since the duty cycle, the lifespan and the population of similar objects are currently poorly known, it is not possible at this stage to quantify their contribution.

Methods

X-ray observations and long-term light curve. We consider in this work X-ray observations taken with Chandra, XMM-Newton and the Neil Gehrels Swift Observatory (see Supplementary Table 1). Particular care is dedicated to the Chandra observation 20830, taken on 6 November 2017, in which we detected diffuse emission. We used the other datasets to build the long-term light curve of Fig. 1 and/or to improve the astrometry of observation 20830.

Chandra. All Chandra observations we used were carried out with the Advanced CCD Imaging Spectrometer[33] (spectroscopic array, ACIS-S) in full-imaging mode. We used the Chandra Interactive Analysis of Observation (CIAO, v4.10)[34] software package and CalDB (v4.7.8)[35]. We selected photons in the energy range 0.3–7 keV, and followed the standard analysis threads for data reprocessing, source detection and flux estimation. We determined the energy boundaries on the basis of the spectral distribution of the ACIS background, which increases significantly outside this band. We defined a circular source region that includes all photons within 3 arcsec from the direction of ULX1. This radius, which contains 98.5% of the PSF, limits the contamination from background and other sources, but is large enough to make it possible to appreciate the main features of the X-ray source. We defined an annular background region centred on the location of ULX1, with radii of 10 arcsec and 30 arcsec. We removed from this region circles with radii of 5 arcsec around each other source, and a circle with a radius of 10 arcsec around NGC 5907 ULX-2, being particularly bright at the time. For observation 20830, these criteria leave 25 photons in the source region and 277 photons in the background region, corresponding to 3.6 background photons expected in the source region (see Supplementary Fig. 1).

XMM-Newton. In the XMM-Newton observations, the positive–negative junction[36] (pn) and the two metal–oxide–semiconductor[37] (MOS) CCD (charge-coupled device) cameras of the EPIC instrument were all operated in full frame mode. We used the XMM-Newton Science Analysis Software[38] (SAS) v14.5 for data reduction. After removing intervals of high background, we selected the events setting FLAG ≡ 0 and PATTERN ≤ 4 and PATTERN ≤ 12 for pn and MOS, respectively. We extracted the source spectra and event lists from a circular region with a radius of 30 arcsec around the best-fit Chandra source position, RA = 228.994289° and dec = 56.302851° (J2000), in the energy range 0.3–10 keV. We estimated the background from a circular region with a radius of 65 arcsec, close to ULX1 but free of sources, for each observation. We excluded from our analysis the XMM-Newton observation 0795712601 as source contamination, mainly from NGC 5907 ULX-2 but also from other sources in NGC 5907, undermines a clear characterization of ULX1[39].

We simultaneously analysed all XMM-Newton spectra in the energy range 0.3–10 keV and fitted them with an absorbed broken power law model (bknpow in XSPEC[40]). The Tübingen–Boulder ISM absorption model (tbabs) was adopted and the abundances were set to those of ref. [41]. We fixed the values of the break energy and the high-energy spectral index to those obtained in ref. [5] ($E_b = 6.7$ keV and $\Gamma_2 = 2.9$), as they were better constrained, including NuSTAR data and consistent with all the XMM-Newton observations of ULX1 in a high state. We also fixed the column density to the best-fit value in ref. [5], $N_H = 5.3 \times 10^{21}$ cm^{-2}. We left the low-energy photon index and the normalization free to vary. We obtained an acceptable fit $\chi^2_\nu = 1.12$ (for 439 degrees of freedom), with low-energy photon indices

of $\Gamma_1^{(2)} = 1.72 \pm 0.03$, $\Gamma_1^{(3)} = 1.88 \pm 0.04$, $\Gamma_1^{(4)} = 1.90 \pm 0.06$, $\Gamma_1^{(5)} = 2.82 \pm 0.18$ and $\Gamma_1^{(6)} = 2.08 \pm 0.07$ for the five observations, in chronological order (the superscripts refer to the observation codes in Supplementary Table 1). The resulting 0.3–10 keV unabsorbed fluxes are $F_X^{(2)} = (7.09 \pm 0.15) \times 10^{-13}$ erg cm^{-2} s^{-1}, $F_X^{(3)} = (4.22 \pm 0.10) \times 10^{-13}$ erg cm^{-2} s^{-1}, $F_X^{(4)} = (1.92 \pm 0.07) \times 10^{-13}$ erg cm^{-2} s^{-1}, $F_X^{(5)} = (9.2 \pm 1.2) \times 10^{-14}$ erg cm^{-2} s^{-1} and $F_X^{(6)} = (1.65 \pm 0.07) \times 10^{-13}$ erg cm^{-2} s^{-1} (see Fig. 1). All these uncertainties are at the 90% confidence level. A careful spectral characterization, to be compared with other spectral analyses in the literature, goes beyond the scope of this paper.

Swift. The X-ray telescope[42] (XRT) on board Swift uses a CCD detector sensitive to photons with energies between 0.2 and 10 keV. All observations analysed in this work were performed in imaging photon counting mode. We used FTOOLS[43] v6.15 for standard data processing. We extracted the source events within a radius of 20 arcsec from the Chandra position of ULX1, and evaluated the background in a source-free circular region of radius 130 arcsec, avoiding the plane of NGC 5907. The ancillary response files generated with xrtmkarf account for different extraction regions, vignetting and point-spread function corrections. We used the latest available spectral redistribution matrix (v014). We converted the source rate to 0.2–10 keV luminosity by assuming a distance $D = 17.1$ Mpc and an absorbed broken power-law spectral model with indices 1.57 and 2.87, and break energy 6.42 keV. These are the best-fit parameters obtained in the high state of ULX1[5], consistent with, but more constrained, than the values obtained in the spectral analysis described in the previous section.

As the region around ULX1 is rich of X-ray sources from NGC 5907, which Chandra can resolve but Swift cannot, XRT observations are likely affected by source contamination. A dedicated analysis that addresses this issue is not straightforward and goes beyond the scope of this paper.

Analysis of the Chandra observation of diffuse emission around ULX1. *Relative astrometry.* We considered Chandra observations 12987 and 20994, besides observation 20830. We reprocessed the data, extracted images and run the CIAO task wavdetect, following the indications in the Chandra analysis threads. We selected the sources within 1 arcmin from the nominal position of ULX1, excluding ULX1 itself. We found the translations that best map the coordinates of the sources in observations 12987 and 20994 to those in observation 20830, using the CIAO task wcs_match. We applied these corrections (measuring 0.13 arcsec and 0.30 arcsec, respectively) to the images and aspect solutions of observations 12987 and 20994 and launched again the task wavdetect. The localization of ULX1 in the two observations is now compatible within 1σ in RA ($|\Delta\mathrm{RA}| = 0.06$ arcsec) and dec ($|\Delta\mathrm{dec}| = 0.06$ arcsec), in the relative frame of observation 20830. Therefore, we take the barycentre of these two positions as the (J2000) nominal position of ULX1: RA = 228.994289(8)° and dec = 56.302851(4)° (or RA = 15 h 15 min 58.63 s, dec = +56° 18′ 10.3″). The best fit coordinates of the closest source to ULX1 in observation 20830 are: RA = 228.99414(11)° and dec = 56.30284(6)° (J2000). These two positions are compatible within 2σ, being offset by 0.3 arcsec, with a 1σ uncertainty of 0.21 arcsec. Therefore, we identify the source in observation 20830 with ULX1 and adopt the nominal position of ULX1 in the analysis that follows.

Extension. A first indication of source extension comes from the output of the CIAO tool wavdetect. We tested for and measured the extension of our source, by studying its radial brightness profile. We used a Kolmogorov–Smirnov test, which quantifies the goodness of fit by measuring the maximum absolute difference between the cumulative distribution of observed events and the model. To take into account the complex shape of the PSF and other effects due to the spacecraft dithering, we simulated with MARX[44] (v5.3.3) a large number of events associated to a point source with characteristics similar to ULX1 in observation 20830, including its position on the detector. To avoid photon pile-up, which alters the PSF, we generated 50 realizations of a source with 1,000 events and combined them. We assumed an absorbed ($N_H = 5.3 \times 10^{21}$ cm^{-2}, the value measured for ULX1 in the high state[5]), power-law ($\Gamma = 2$) spectrum and a direction consistent with those of ULX1. We obtain consistent results assuming the best-fit thermal bremsstrahlung spectral model described in the next section. We generated a number of simulated background events, drawing from a two-dimensional uniform distribution.

We extracted the observed cumulative distribution of events within a radius R from the source centre. We used the nominal direction of ULX1 obtained through astrometric analysis (see the previous section), but using the observed centroid does not alter our results. For the simulated point source, we included the expected uniform background contribution. We applied the same selection criteria to the simulated data set and considered only photons in the source region (with a radius of 3 arcsec): 25 observed photons compared against 4×10^4 simulated photons.

A Kolmogorov–Smirnov test finds a maximum difference between the two cumulative radial distributions, $D = 0.525$ (Fig. 2). This implies that the source associated to ULX1 is not pointlike with a confidence level of 5σ (P value $= 3 \times 10^{-7}$). We repeated the same analysis simulating extended sources with a disk profile of uniform surface brightness. We can reject at the 2σ confidence level all values of the disk radius outside the range $R_d = 1.35 \pm 0.50$ arcsec. We repeated the same analysis assuming a smooth halo shape[45] with a hole, as described in the section of the Supplementary Information where we apply a dust scattering model. We constrained the values of the distance between the source and a dust layer to $d_{sd} = 11 \pm 5$ kpc. In the spirit of reproducible results, we provide the code of the MARX plugin (Draine_halo.c) that we used to simulate such a dust halo at https://github.com/andrea-belfiore/MARX-plugins.git.

Spectral analysis. We analysed the spectrum of the extended source with XSPEC, adopting a collisional plasma model (apec), absorbed according to the Tübingen–Boulder absorption model (tbabs) and set the abundances to those of ref. [41]. As the number of events is very low, we used C-statistics[46] and verified that we obtain identical estimates and error bars using Monte Carlo simulations similar to those described in the previous section. All the uncertainties are stated at 90% CL. The absorption column is poorly constrained by the data (see Supplementary Fig. 2), but physical constraints are given by the absorption level of our Galaxy in the direction of ULX1, $N_{H,G} = 1.2 \times 10^{20}$ cm^{-2}, and the absorption measured in the high state of ULX1, $N_{H,U} = 5.3 \times 10^{21}$ cm^{-2} (which includes internal absorption by the ULX itself). We repeated the same analysis adopting the best-fit value $N_H = 1.3 \times 10^{21}$ cm^{-2}, which provided us with the best-fit estimates for all parameters, and for the two extreme values $N_{H,G}$ and $N_{H,U}$ that determine our uncertainties (that cover the 90% CL error bars for all allowed values of N_H).

We estimate a characteristic energy $k_B T = 1.9^{+2.3}_{-0.8}$ keV, a normalization $N = 3.5^{+2.5}_{-1.9} \times 10^{-6}$, and an unabsorbed 0.3–7.0 keV flux $F_X = 6.1^{+6.1}_{-2.5} \times 10^{-15}$ erg cm^{-2} s^{-1}, corresponding to an isotropic 0.3–7.0 keV luminosity $L_X = 2.1^{+2.1}_{-0.9} \times 10^{38}$ erg s^{-1}.

We also tested through Monte Carlo simulations a dust-scattering spectrum expected from the model outlined in a following section. This model is acceptable at the 2σ level (the spectrum changes so slightly with the tuning parameters that we cannot constrain them in this way).

We try to estimate the flux of a point-like component associated to ULX1. To this aim, we consider only the innermost photons, within 0.5 arcsec from the location of ULX1, determined as described in the astrometry section. We assume for the point source a power-law spectrum with $\Gamma = 2$ and the absorption column $N_{H,U} = 5.3 \times 10^{21}$ cm^{-2} measured for ULX1 in its high state. We used the CIAO tool srcflux, that applies an aperture photometry, taking into account the response of the instrument, the encircled fraction (fraction of the PSF within each region), statistical uncertainties, position on the detector and other effects. It provides an upper limit on the flux (at the 90% confidence level) of $F_X < 3.4 \times 10^{-15}$ erg cm^{-2} s^{-1}. This corresponds to a luminosity $L_X < 1.2 \times 10^{38}$ erg s^{-1} $= 0.68 L_{14}$, where $L_{14} = 1.764 \times 10^{38}$ erg s^{-1} is the Eddington limit for a $1.4\,M_\odot$ neutron star.

Physical modelling of the expanding nebula. We assume that an isotropic wind with constant power L_w is emitted from the ULX system, shocks the external medium (ISM) and expands according to a self-similar solution[21,22]. After a short free expansion period, the wind forms a shock that starts as adiabatic but becomes more and more radiatively efficient. In this phase, the expanding nebula (bubble) is radially structured in four regions:

1. Close to the source is the low-density leftovers of the swept-up ISM, where the wind expands freely (free wind region).
2. Starting at a radius R_1 the wind, faster than the shock, accumulates, increasing density and temperature (shocked wind region).
3. Starting at a radius R_c the swept up ISM accumulates, increasing density and temperature (shocked ISM region).
4. Beyond a radius R_2 the ISM is still unperturbed by the shock (ISM region).

In this model, there are two shocked regions where X-rays could be emitted: the shocked wind region and the shocked ISM region. The first scenario was considered in a set of simulations[47] of expanding nebulae, and, with the boundary conditions set in these simulations, it cannot reach an X-ray luminosity larger than ~10^{35} erg s^{-1}. Either this scenario is missing some dominant effect, or it can be ruled out in the context of ULX1; we explore here the other scenario.

If we assume that the X-rays are produced in the shocked ISM region, then the observed disk radius $R_d = 1.35 \pm 0.50$ arcsec coincides with $R_2(\tau) = 112 \pm 42$ pc at a distance $D = 17.1$ Mpc, where τ is the current age of the bubble. Strong shock conditions for the temperature of the shocked ISM provide a direct estimate of the current speed of the shock v_{sh}:

$$v_{sh}^{(0)} = \sqrt{\frac{16}{3}\frac{k_B T}{m_p}} = \left(3.3^{+1.6}_{-0.8}\right) \times 10^{-3} c = \left(9.9^{+4.8}_{-2.4}\right) \times 10^2 \,\mathrm{km\,s^{-1}} \quad (1)$$

Because observations of other nebulae show that the shock speed is somewhat overestimated with this approximation, we introduce a factor $\xi < 1$ that accounts for this discrepancy: $v_{sh} = v_{sh}^{(0)} \times \xi$. A standard bubble model, with a constant injection of mechanical power L_w in a uniform ISM with density n_{ISM}, predicts a time dependence of the bubble size:

$$R_2(t) = \alpha \left(\frac{L_w t^3}{n_{ISM} m_p}\right)^{1/5} \quad (2)$$

where $\alpha = 0.88$ is a numerical constant[22].

Under these assumptions, as $v_{sh} = \frac{dR_2}{dt}$, we can estimate the age of the bubble:

$$\tau = \frac{3}{5}\frac{R_2}{v_{\rm sh}} = \left(6.7^{+3.1}_{-2.8}\right) \times 10^4\,{\rm yr} \times \xi^{-1} \quad (3)$$

As $v_{\rm sh}$ largely exceeds the sound speed in the ISM, the Rankine–Hugoniot conditions at the shock front grant that the plasma density just inside the shocked region is $n_{\rm sh} = W \times n_{\rm ISM}$, with a compression factor $W \simeq 4$. However, as a high radiative efficiency strongly increases this value, we maintain it as a free parameter. According to the standard bubble model, $n_{\rm sh}$ decreases down to 0 as the radial distance r approaches a contact discontinuity at $r = R_{\rm c}$. Because the bremsstrahlung emissivity $\epsilon \propto n_{\rm sh}^2$, we assume that most emission is produced close to R_2. We estimate the size of this emitting region $V_{\rm sh}$ by assuming that it contains most of the swept up material from the ISM:

$$V_{\rm sh} \simeq \frac{4}{3}\pi R_2^3 \frac{n_{\rm ISM}}{n_{\rm sh}} = \left(1.5^{+2.3}_{-1.1}\right) \times 10^6\,{\rm pc}^3 \times \left(\frac{W}{4}\right)^{-1} \quad (4)$$

We can now extract from the normalization of the apec model an estimate of the shocked plasma density as

$$n_{\rm sh} = 3.1^{+11}_{-2.1} \times 10^{-1}\,{\rm cm}^{-3} \times \left(\frac{W}{4}\right)^{\frac{1}{2}} \quad (5)$$

This value is broadly consistent with those observed in optical/radio ULX bubbles[23].

We use equation (2) to provide an estimate of the mechanical power of the wind $L_{\rm w}$:

$$\begin{aligned} L_{\rm w} &= \frac{m_{\rm p} n_{\rm ISM} R_2^5}{\alpha^3 \tau^3} \simeq 108 m_{\rm p} n_{\rm ISM} R_2^2 \left(\frac{k_{\rm B} T}{m_{\rm p}}\right)^{3/2} \times \xi^3 \\ &= \left(1.3^{+9.8}_{-1.0}\right) \times 10^{41}\,{\rm erg\ s^{-1}} \times \xi^3 \times \left(\frac{W}{4}\right)^{-\frac{1}{2}} \end{aligned} \quad (6)$$

where we used equation (1) and (3) and our estimates for $R_{\rm d}$, $k_{\rm B}T$ and $n_{\rm ISM}$, leading to large uncertainties. This value is in the same order of magnitude as the X-ray luminosity observed from ULX1 at its peak, if emitted isotropically[5]. Although $L_{\rm w}$ is weakly constrained from our results, we deem it extremely unlikely that it can be much higher.

Indeed, if we suppose that ULX1 sustained this value of $L_{\rm w}$ for the age of the nebula τ, its wind would have carried an energy $E = L_{\rm w}\tau = \left(2.8^{+18}_{-2.2}\right) \times 10^{53}\,{\rm erg} \times \xi^2 \times \left(\frac{W}{4}\right)^{-\frac{1}{2}}$. As the wind, and therefore the bubble, is powered by accretion onto a neutron star, the accreted mass must be at least:

$$M_{\rm accr} = \frac{E}{\eta c^2} \simeq \left(1.8^{+12}_{-1.5}\right) \times 10^{33}\,{\rm g} = 0.9^{+5.9}_{-0.7}\,{\rm M}_\odot \quad (7)$$

where $\eta \approx \frac{GM_{\rm ns}}{R_{\rm ns}c^2} \approx 17\%$ is the accretion efficiency of a neutron star with mass $M_{\rm ns} = 1.4\,M_\odot$ and radius $R_{\rm ns} = 12\,{\rm km}$. The best-fit value of $M_{\rm accr}$ might be too large for a neutron star, as it would have probably already collapsed into a black hole, but a value of $M_{\rm accr} < 0.5\,M_\odot$ is more plausible. As the accretion power is not all channelled into the wind, but must also sustain the luminosity of ULX1, it seems likely that our simple model might need some revision.

We can relate the total mass ejected by the wind, $M_{\rm w}$ to E and, indirectly, to $M_{\rm accr}$:

$$M_{\rm w} = \frac{2\eta M_{\rm accr} c^2}{v_{\rm w}^2} \quad (8)$$

where $v_{\rm w}$ is the speed of the wind. If we assume $M_{\rm accr} \simeq 0.5\,M_\odot$, then, to keep $M_{\rm w} \lesssim 10\,M_\odot$ as expected for an X-ray binary system, $v_{\rm w} > 0.1c$. This value of $v_{\rm w}$ agrees with the velocity measured in outflows from various ULXs[25–27].

Data availability

The datasets analysed in this work (XMM-Newton OBSIDs: 0804090301, 0804090401, 0804090501, 0804090601, 0804090701; Chandra OBSIDs: 12987, 20830, 20994, 20995) are available for download from the HEASARC archive at https://heasarc.gsfc.nasa.gov. The data that support the plots within this paper and other findings of this study are available from the corresponding author on reasonable request.

Code availability

The code used in this work is available from the corresponding author on reasonable request.

Received: 4 January 2019; Accepted: 30 August 2019;
Published online: 28 October 2019

References

1. Feng, H. & Soria, R. Ultraluminous X-ray sources in the Chandra and XMM-Newton era. *New Astron. Rev.* **55**, 166–183 (2011).
2. Kaaret, P., Feng, H. & Roberts, T. P. Ultraluminous X-ray sources. *Annu. Rev. Astron. Astrophys.* **55**, 303–341 (2017).
3. Bachetti, M. et al. An ultraluminous X-ray source powered by an accreting neutron star. *Nature* **514**, 202–204 (2014).
4. Fürst, F. et al. Discovery of coherent pulsations from the ultraluminous X-ray source NGC 7793 P13. *Astrophys. J. Lett.* **831**, L14 (2016).
5. Israel, G. L. et al. An accreting pulsar with extreme properties drives an ultraluminous X-ray source in NGC 5907. *Science* **355**, 817–819 (2017).
6. Israel, G. L. et al. Discovery of a 0.42-s pulsar in the ultraluminous X-ray source NGC7793 P13. *Mon. Not. R. Astron. Soc.* **466**, L48–L52 (2017).
7. Carpano, S., Haberl, F., Maitra, C. & Vasilopoulos, G. Discovery of pulsations from NGC 300 ULX1 and its fast period evolution. *Mon. Not. R. Astron. Soc.* **476**, L45–L49 (2018).
8. Drury, L. O. Origin of cosmic rays. *Astropart. Phys.* **39**, 52–60 (2012).
9. Abeysekara, A. U. et al. Very-high-energy particle acceleration powered by the jets of the microquasar SS 433. *Nature* **562**, 82–85 (2018).
10. Xilouris, E. M., Byun, Y. I., Kylafis, N. D., Paleologou, E. V. & Papamastorakis, J. Are spiral galaxies optically thin or thick? *Astron. Astrophys.* **344**, 868–878 (1999).
11. Tully, R. B. et al. Cosmicflows-2: the data. *Astron. J.* **146**, 86 (2013).
12. Just, A., Möllenhoff, C. & Borch, A. An evolutionary disc model of the edge-on galaxy NGC 5907. *Astron. Astrophys.* **459**, 703–716 (2006).
13. Blondin, J. M., Wright, E. B., Borkowski, K. J. & Reynolds, S. P. Transition to the radiative phase in supernova remnants. *Astrophys. J.* **500**, 342–354 (1998).
14. Fryer, C. L. et al. Compact remnant mass function: dependence on the explosion mechanism and metallicity. *Astrophys. J.* **749**, 91 (2012).
15. Barkov, M. V. & Komissarov, S. S. Recycling of neutron stars in common envelopes and hypernova explosions. *Mon. Not. R. Astron. Soc.* **415**, 944–958 (2011).
16. Pakull, M. W. & Mirioni, L. Optical counterparts of ultraluminous X-ray sources. Preprint at https://arxiv.org/abs/astro-ph/0202488 (2002).
17. Pakull, M. W. & Mirioni, L. Bubble nebulae around ultraluminous X-ray sources. *Rev. Mex. Astron. Astrofis.* **15**, 197–199 (2003).
18. Pakull, M. W. & Grisé, F. in *A Population Explosion: The Nature and Evolution of X-ray Binaries in Diverse Environments* (eds Bandyopadhyay, R. M. et al.) 303–307 (AIP, 2008).
19. Lang, C. C., Kaaret, P., Corbel, S. & Mercer, A. A radio nebula surrounding the ultraluminous X-ray source in NGC 5408. *Astrophys. J.* **666**, 79–85 (2007).
20. Kaaret, P., Corbel, S., Prestwich, A. H. & Zezas, A. Radio emission from an ultraluminous X-ray source. *Science* **299**, 365–368 (2003).
21. Castor, J., McCray, R. & Weaver, R. Interstellar bubbles. *Astrophys. J.* **200**, L107–L110 (1975).
22. Weaver, R., McCray, R., Castor, J., Shapiro, P. & Moore, R. Interstellar bubbles. II – Structure and evolution. *Astrophys. J.* **218**, 377–395 (1977).
23. Pakull, M. W., Soria, R. & Motch, C. A 300-parsec-long jet-inflated bubble around a powerful microquasar in the galaxy NGC 7793. *Nature* **466**, 209–212 (2010).
24. Dopita, M. A., Payne, J. L., Filipović, M. D. & Pannuti, T. G. The physical parameters of the microquasar S26 in the sculptor group galaxy NGC 7793. *Mon. Not. R. Astron. Soc.* **427**, 956–967 (2012).
25. Pinto, C., Middleton, M. J. & Fabian, A. C. Resolved atomic lines reveal outflows in two ultraluminous X-ray sources. *Nature* **533**, 64–67 (2016).
26. Kosec, P. et al. Evidence for a variable ultrafast outflow in the newly discovered ultraluminous pulsar NGC 300 ULX-1. *Mon. Not. R. Astron. Soc.* **479**, 3978–3986 (2018).
27. Walton, D. J. et al. An iron K component to the ultrafast outflow in NGC 1313 X-1. *Astrophys. J.* **826**, L26 (2016).
28. Rand, R. J. Diffuse ionized gas in nine edge-on galaxies. *Astrophys. J.* **462**, 712 (1996).
29. Mezcua, M., Roberts, T. P., Sutton, A. D. & Lobanov, A. P. Radio observations of extreme ULXs: revealing the most powerful ULX radio nebula ever or the jet of an intermediate-mass black hole? *Mon. Not. R. Astron. Soc.* **436**, 3128–3134 (2013).
30. Dopita, M. A. & Sutherland, R. S. Spectral signatures of fast shocks. I. Low-density model grid. *Astrophys. J. Suppl. Ser.* **102**, 161–188 (1996).
31. Caplan, J. & Deharveng, L. Extinction and reddening of H II regions in the large magellanic cloud. *Astron. Astrophys.* **155**, 297–313 (1986).
32. Begelman, M. C., King, A. R. & Pringle, J. E. The nature of SS433 and the ultraluminous X-ray sources. *Mon. Not. R. Astron. Soc.* **370**, 399–404 (2006).
33. Garmire, G. P., Bautz, M. W., Ford, P. G., Nousek, J. A. & Ricker, G. R. Jr. Advanced CCD imaging spectrometer (ACIS) instrument on the Chandra X-ray observatory. *Proc. SPIE* **4851**, 28–44 (2003).
34. Fruscione, A. et al. CIAO: Chandra's data analysis system. *Proc. SPIE* https://doi.org/10.1117/12.671760 (2006).
35. CalDB 4.8.4 (Chandra X-ray Center, 2019); https://go.nature.com/2naVcgC
36. Strüder, L. et al. The European photon imaging camera on XMM-Newton: the pn-CCD camera. *Astron. Astrophys.* **365**, L18–L26 (2001).

37. Turner, M. J. L. et al. The European photon imaging camera on XMM-Newton: the MOS cameras. *Astron. Astrophys.* **365**, L27–L35 (2001).
38. Gabriel, C. et al. The XMM-Newton SAS - distributed development and maintenance of a large science analysis system: a critical analysis. In *Astronomical Data Analysis Software and Systems (ADASS) XIII* (eds Ochsenbein, F. et al.) 759–763 (ASP, 2004).
39. Pintore, F. et al. A new ultraluminous X-ray source in the galaxy NGC 5907. *Mon. Not. R. Astron. Soc.* **477**, L90–L95 (2018).
40. Arnaud, K. A. XSPEC: the first ten years. In *Astronomical Data Analysis Software and Systems V* (eds Jacoby, G. H. & Barnes, J.) 17–20 (ASP, 1996).
41. Wilms, J., Allen, A. & McCray, R. On the absorption of X-rays in the interstellar medium. *Astrophys. J.* **542**, 914–924 (2000).
42. Burrows, D. N. et al. The swift X-ray telescope. *Space Sci. Rev.* **120**, 165–195 (2005).
43. Blackburn, J. K. FTOOLS: a fits data processing and analysis software package. In *Astronomical Data Analysis Software and Systems IV* (eds Shaw, R. A. et al.) 367–370 (ASP, 1995).
44. Davis, J. E. et al. Raytracing with MARX: X-ray observatory design, calibration, and support. *Proc. SPIE* https://doi.org/10.1117/12.926937 (2012).
45. Draine, B. T. Scattering by interstellar dust grains. II. X-rays. *Astrophys. J.* **598**, 1026–1037 (2003).
46. Cash, W. Parameter estimation in astronomy through application of the likelihood ratio. *Astrophys. J.* **228**, 939–947 (1979).
47. Siwek, M., Sadowski, A., Narayan, R., Roberts, T. P. & Soria, R. Optical and X-ray luminosities of expanding nebulae around ultraluminous X-ray sources. *Mon. Not. R. Astron. Soc.* **470**, 361–371 (2017).
48. Walton, D. J. et al. A 78 day X-ray period detected from NGC 5907 ULX1 by swift. *Astrophys. J.* **827**, L13 (2016).

Acknowledgements

This research is based on observations made with the Chandra X-ray Observatory and has made use of software provided by the Chandra X-ray Center (CXC) in the application packages CIAO, ChIPS and Sherpa. This research also made use of data obtained with the Neil Gehrels Swift Observatory and XMM-Newton. Swift is a NASA mission with participation of the Italian Space Agency and the UK Space Agency. XMM-Newton is an ESA science mission with instruments and contributions directly funded by ESA Member States and NASA. A.B. is grateful to A. Fabian for an interesting discussion and to S. Covino for help in optical data reduction. A.B. and G.N. are supported by EXTraS, a project funded by the European Union's Seventh Framework Programme under grant agreement no. 607452. We acknowledge funding in the framework of the project ULTraS (ASI-INAF contract no. 2017-14-H.0). M.M. acknowledges funding from ASI-INAF contract no. 2015-023-R.0. D.J.W. acknowledges financial support from an STFC Ernest Rutherford Fellowship.

Author contributions

A.B., A.T., F.P., G.N. and P.E. processed and analysed the data. A.B. and D.M. performed the statistical analysis. Theoretical interpretation was mainly provided by A.B. with contributions and inputs by A.D.L., A.T., F.P., P.E., R.S. and other co-authors. A.B. and P.E. composed the text. All authors discussed the results and commented on the manuscript.

Competing interests

The authors declare no competing interests.

Additional information

Supplementary information is available for this paper at https://doi.org/10.1038/s41550-019-0903-z.

Correspondence and requests for materials should be addressed to A.B.

Reprints and permissions information is available at www.nature.com/reprints.

Publisher's note Springer Nature remains neutral with regard to jurisdictional claims in published maps and institutional affiliations.